

Scalar gradient behaviour in MILD combustion

Y. Minamoto and N. Swaminathan
Department of Engineering, University of Cambridge
Cambridge, UK

1 Introduction

Combustion systems are constantly improved to achieve high efficiency and low emissions simultaneously. Moderate and intense low-oxygen dilution (MILD) or “flameless” combustion is a potential technology to achieve these requirements. In MILD conditions [1–3], the reactant temperature, T_r , is higher than the autoignition temperature of a given mixture, and the temperature rise during combustion, $\Delta T = T_p - T_r$, is smaller than the autoignition temperature. In order for the second condition to be met, the reactant mixture is highly diluted with the exhaust gas. This gives a typical oxygen molar fraction in reactant mixture of $X_{O_2,r} \sim 0.02 - 0.05$. There are number of benefits from MILD combustion. First the combustion efficiency is enhanced due to the high preheating temperature [1–3]. Second, the pollutant emissions or thermal NO formation is suppressed significantly because of the low flame temperature and the low oxygen levels available for combustion [1–3]. Also, combustion noise and instabilities are significantly suppressed because of the small temperature rise. MILD combustion is represented using a combustion type diagram as shown in Fig. 1a. The conditions of three cases considered in this study are also shown. All of these cases have the same equivalence ratio $\phi = 0.8$, but the reactants for Flame A and Flame B are diluted to have respectively $X_{O_2,r} = 0.048$ and 0.035 with H_2O and CO_2 , while Flame C has undiluted mixture, $X_{O_2,r} = 0.194$. These three cases clearly represent respectively MILD and conventional premixed combustion conditions in the diagram. The temperature profile shown in Fig. 1b for the one-dimensional MILD and conventional premixed flames shows that the MILD case has very small temperature gradients compared to the conventional flame.

Recent studies using laser diagnostics [4, 5] for OH and temperature fields suggest that reaction zones are distributed in MILD combustion. This questions the use of flamelet based modelling approaches for RANS or LES simulations of MILD combustion. Generally, a direct measurement of spatial variation of heat release or reaction rate is not easy using laser diagnostics. However, it is a common practice to infer heat release rate variation using representative and specific species concentrations detected using laser diagnostics [6–8] for species molar concentrations such as [CH], [CHO], [CH_2O] and [OH]. In the past, PLIF signals such as S_{CH} , S_{CHO} , and the product of PLIF signals, $S_{OH} \times S_{CH_2O}$ are used for conventional flames [6–8]. For MILD combustion, however, S_{CH} and S_{CHO} may not be suitable choices since their SN ratio is generally low. The simultaneous PLIF imaging of S_{OH} and S_{CH_2O} is possible because of high SN ratio and it has been done quite commonly in laser diagnostics studies of turbulent flames [6, 9].

The objectives of this study are (i) to show that $S_{OH} \times S_{CH_2O}$ has a reasonable correlation with the heat release rate field even for MILD combustion conditions, and (ii) to investigate the scalar gradient probability density function (PDF) obtained using PLIF images which are deduced from three-dimensional

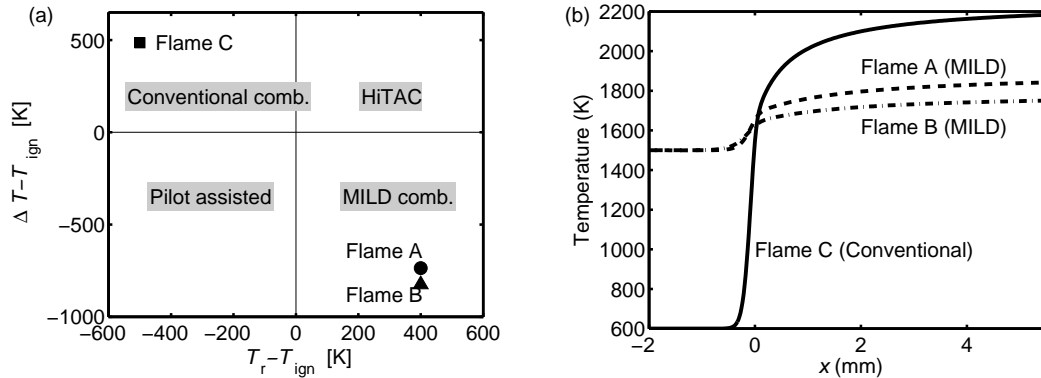


Figure 1. A diagram showing combustion types [3] (a) and temperature variations in laminar MILD and conventional flames ($x = 0$ is the location of the peak heat release rate) (b).

direct numerical simulation (DNS) results. The numerical method used for the DNS results is discussed briefly along with a summary of conditions in Sec. 2. The DNS results are presented in Sec. 3. The scalar gradient PDF is studied in Sec. 4.

2 Numerical method and combustion conditions

In this study, MILD and planar turbulent premixed methane-air combustion conditions with diluted and undiluted reactants are considered using DNS methodology. Compressible transport equations are solved on uniform mesh for mass, momentum, internal energy, and mass fractions. The transport properties are temperature dependent, and combustion kinetics is modelled using a skeletal mechanism involving 16 species with non-unity Lewis numbers. A tenth order central difference scheme for spatial and a third order Runge-Kutta scheme for temporal derivatives are used. The computational domain is cubic with non-reflecting in- and out-flow boundaries in x , and periodic boundaries in y and z directions. The construction of initial and inlet mixture field for MILD combustion simulation is important, since it has to account for mixing phenomena observed in MILD combustion devices employing technologies such as EGR, FGR and staged fuel injection. Thus, a partially premixed mixture of burnt and unburnt gases preheated using recovered exhaust heat are carefully constructed following the steps reported in Minamoto *et al.* [10]. The initial and inlet mixture field consists of all the species including radicals. These inlet species mass fractions are varied temporary and spatially. This mixture has a small mixture fraction fluctuation of about $\pm 5\%$ of its mean value of 0.01 (Case A) and 0.008 (Case B). The variance of a reaction progress variable field based on the fuel mass fraction is about 0.09 with a mean value of 0.5. Temperature also fluctuates within $\pm 5\%$ of the mean temperature, 1500 K due to the mixing process. For the premixed case, the preheat temperature is uniform and is 600 K. The inlet mixture field for the MILD and premixed cases is fed into the DNS domain at the mean velocity of U_{in} . Table 1 shows combustion and turbulence conditions of various cases considered in this study. The dilution levels are shown as the maximum and spatial average of O_2 molar fraction denoted respectively by $X_{O_2,r}^{max}$ and $\langle X_{O_2,r} \rangle$. The laminar flame speed, S_L , Zeldovich thickness, δ_F , and thermal thickness, δ_{th} , are obtained from the planar laminar flame calculations. Please note that the mixture composition of the canonical laminar flames for the MILD cases is based on the spatially averaged mass fraction for major species in the DNS initial field. Such canonical flame is found to well represents the burnt temperature in the 3D DNS field. Also, since the diluted reactant mixture of this canonical flame contains only CH_4 , O_2 , H_2O and CO_2 unlike the DNS initial field, the reaction rate at inlet boundary during 1D flame cal-

Table 1. Thermochemical and turbulence conditions.

Case	$X_{O_2,r}^{\max}$	$\langle X_{O_2,r} \rangle$	S_L (m/s)	δ_F (mm)	U_{in}/S_L	u'/S_L	l_0/δ_F	l_0/δ_{th}	Re_{l_0}	Da
MILD A	0.048	0.035	2.62	0.138	9.6	3.80	12.3	1.70	67.0	3.25
MILD B	0.035	0.025	1.66	0.217	15.1	9.88	6.8	1.15	96.1	0.69
Premixed	0.194	0.194	2.57	0.064	3.0	2.19	12.3	2.11	38.5	5.64

ulation is sufficiently small to carry out one-dimensional flame calculation, even with high preheating temperature conditions. The root mean square of turbulent velocity fluctuations, u' , its integral length scale, l_0 , and Reynolds number based on l_0 are for the preprocessed inflowing mixture. The Damköhler number, Da, is defined as $Da = (l_0/\delta_F)/(u'/S_L)$. The computational domain has a dimension of $L_x \times L_y \times L_z = 10 \times 10 \times 10 \text{ mm}^3$ for the MILD cases, and $10 \times 5 \times 5 \text{ mm}^3$ for the premixed case. The domains are discretised using 512^3 and 384^3 mesh points for the MILD cases, respectively Cases A and B, and $512 \times 256 \times 256$ mesh points for the premixed case. These numerical resolution ensures that there are at least 15 mesh points inside δ_{th} . In order to minimise the effect of initial transients, the simulation was first run for 1.5 flow through time τ_D , which is the mean convection time from the inlet to outlet boundaries, for the MILD cases and one τ_D for the premixed case. After these periods, the data is sampled over one τ_D and $0.56 \tau_D$ to collect 80 and 93 data sets for the MILD and premixed cases respectively.

3 Reaction zone structure

The x - y slice of normalised reaction rate of progress variable based on temperature, $\omega_{c_T}^*$, is shown for the MILD B and the premixed cases in Figs. 2 (a) and (b). Here the superscript “*” denotes a normalisation using the global maximum value in the respective two-dimensional slice, and the superscript “+” denotes an appropriate normalisation using the laminar flame quantities, ρ_r , S_L and δ_{th} , where ρ_r is the density of reactants. Contours of the progress variable based on temperature, c_T , are also shown for $c_T = 0.4, 0.6$ and 0.8 . These snapshots are taken at $t = 1.5\tau_D$ and $z = 0.5L_z$ for both cases. The spatial variation of $\omega_{c_T}^*$ shows the nature of the heat release rate in the MILD B case compared to the premixed case. Because of the non-uniformity in the mixture and relatively high turbulence level, the reaction zones look more convoluted and distributed in the MILD case compared to the premixed case. The degree of convolution in the MILD A (not shown) seems smaller than in MILD B, although reaction zone interactions are observed occasionally. The typical reaction zone thickness (coloured area) in the premixed case is about δ_{th} . The typical thickness of non-interacting reaction zones is also about δ_{th} in the MILD case, and the reaction zones seem to be thickened due to interaction events.

The reaction progress variable variation overlaid in Figs. 2(a) and (b) shows non-flamelet features in the MILD case. In the premixed case, the local peak of heat release rate is always located at around $c_T = 0.6$. The two iso-contours of $c_T = 0.4$ and 0.8 are always parallel and follow 0.6 contour closely, suggesting a thin-sheet like structure for the reaction zones with strong scalar gradients. On the other hand, the iso-contours of c_T in the MILD case do not always show such a relation between $\omega_{c_T}^*$ and c_T . The intense reaction regions do not always locate at a particular c_T and there seems no preferential regions in the domain for the intense reaction. Contours of $c_T = 0.4$ and 0.8 are not parallel and the distance between them suggests a very small c_T gradient compared to the premixed flame. However, there are regions where c_T and intense reaction rate are aligned as in the premixed case, implying flamelet like combustion. Such co-existence of flamelet and non-flamelet like reaction zones is due to the inhomogeneous and diluted mixture field.

Figures 2(c) and (d) show the product field, $\omega_{est}^* = (S_{OH} \times S_{CH_2O})^*$ for both cases considered. Here, the PLIF signals are deduced as $S_{CH_2O} = [CH_2O]T^{1-\alpha}$ and $S_{OH} = [OH]T^{1-\beta}$, where $\alpha = 2.6$ and

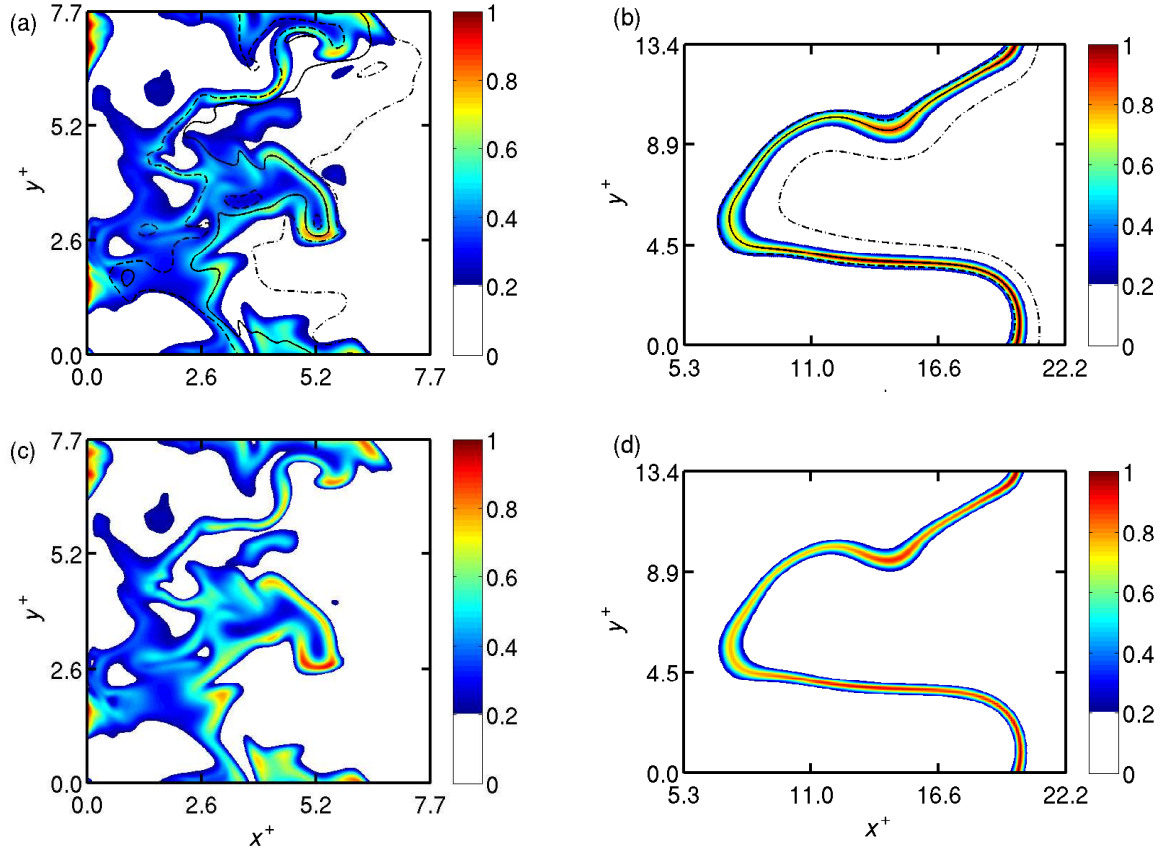


Figure 2. Spatial variations of $\omega_{c_T}^*$ (colour) and c_T (lines) in the mid x - y plane at $t = 1.5\tau_D$ for the MILD B (a) and the premixed (b) cases. Dashed line: $c_T = 0.4$, solid line: 0.6, and dash-dotted line: 0.8. Spatial variation of ω_{est}^* is also shown for the MILD B (c) and the premixed (d) cases.

$\beta = 0$ are used, considering temperature dependence of the signals [6]. However, the parameters, α and β , are found not to unduly change the conclusions in this study. Although there are local differences compared to Figs. 2(a) and (b), the overall reaction zone shapes are reasonably captured for both cases. The typical thickness of non-interacting reaction zones are also well represented by the product field. Therefore the conventional method to estimate the heat release rate using ω_{est} , is also applicable for the MILD combustion.

4 Conditional PDF of scalar gradient using PLIF images deduced from DNS

The scalar gradient PDF conditioned on the reaction rate is investigated to further insights into the flamelet or non-flamelet behaviour of the MILD combustion. For classical turbulent combustion with thin reaction zones, the flame normal component of a scalar gradient is very large compared to the tangential component. Hence statistically the relation between the normal component of the scalar gradient and the reaction rate in the turbulent premixed combustion would be close to that of the respective laminar flame. However, since three-dimensional scalar measurements are not generally easy to carry out, two-dimensional scalar gradients are considered for this study. The normal and tangential directions, and the scalar gradient are calculated here based on the local reaction rate, ω_{est} , and a progress variable, $c_{est} = S_{OH}/S_{OH,max}$, respectively. Although c_{est} distribution cannot be fully representative of

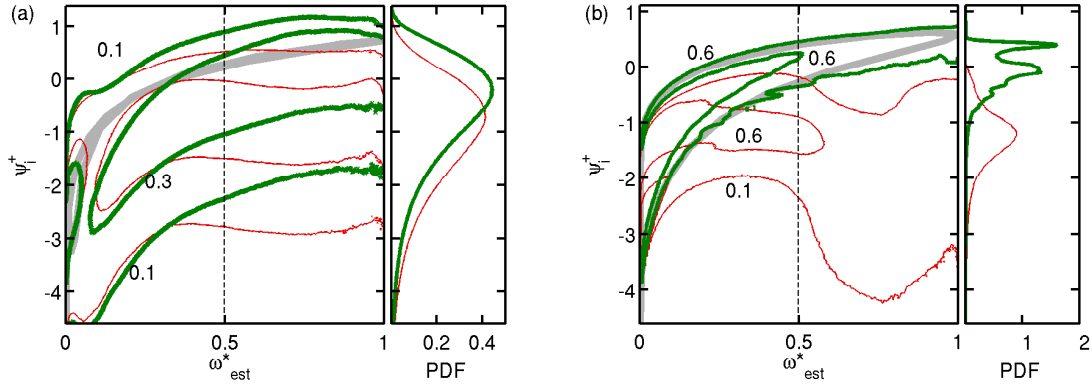


Figure 3. The PDF of ψ_1 (thick green line) and ψ_2 (thin red line) conditioned on estimated reaction rate, ω_{est}^* , for MILD B (a) and the premixed case (b). The grey thick line is the respective laminar flame solution, $(\psi_1^+, \omega_{est}^*)$. The PDF shown in the right subset is $P(\psi_i^+ | \omega_{est}^* = 0.50)$.

the actual progress variable field since [OH] behaviour is non-monotonic with respect to c_T , the local direction of c_{est} gradient obtained at the deduced reaction zones is found to be close to that of the actual progress variable gradient.

The conditional scalar gradient PDF is constructed as follows. The reaction surface is identified using the local minimum value of $\nabla\omega_{est}^*$ subject to $\omega_{est}^* > \omega_{est,1}$, where $\omega_{est,1} = 0.5$. This surface is then expressed as $(f_x(s), f_y(s))$ for a particular 2D plane, where s is a local coordinate on the surface. The normal vector, \mathbf{n}_1 , of the surface is first calculated as $\mathbf{n}_1 = (-df_y/ds, df_x/ds)$ for the 2D plane. The similar procedures are followed for the tangential vector, \mathbf{n}_2 . The samples required to construct the gradient PDFs are collected along either in normal or tangential directions for $\pm 2\delta_{th}$. The scalar gradients are transformed into logarithmic scale as $\psi_i^+ = \ln(\nabla c_{est}^+ \cdot \mathbf{n}_i)$, due to the log-normality of the scalar gradient, and the conditional PDF is obtained from the joint PDF using $P(\psi_i^+ | \omega_{est}^*) = P(\psi_i^+, \omega_{est}^*) / P(\omega_{est}^*)$.

Figure 3 shows the conditional PDF for the normal and tangential components. A comparison of the laminar flame solution and the conditional PDF for the premixed case shows that the most probable normal scalar gradient agrees with the laminar flame solution suggesting the flamelet combustion. However, for the MILD case, such an agreement in the normal scalar gradient is not observed. Moreover, the PDF is relatively broad compared to the premixed case. A close study of the subset PDF, where PDF of the scalar gradient is shown for $\omega_{est}^* = 0.5$, the difference in the PDF peak locations for the normal and tangential components is much smaller in the MILD case than in the premixed case. This signifies weaker directional features of the scalar gradient in the MILD B case. The conditional PDF in Fig. 3a suggests that reaction zone behaviour is less flamelet like in the MILD case in a statistical sense, although the gradient somehow increases with the reaction rate, suggesting flamelet like behaviour for MILD combustion. Similar scalar gradient behaviour is observed in the other MILD case as well (not shown). Similar conditional PDF using 3D scalar gradient calculated from the actual progress variable and the actual heat release rate is also constructed for these cases (not shown in this paper, but will be discussed in the presentation). A comparison of the conditional PDFs from the 3D field to those obtained from the deduced PLIF images, shown in Fig. 3, suggests that the later PDFs can capture the scalar gradient behaviour of both cases as much as the former full 3D PDF can do. The PDF constructed here would be also useful in both numerical and experimental studies to investigate flamelet and non-flamelet behaviour of turbulent flames in general.

5 Summary

Scalar gradient behaviour in diluted (MILD) and undiluted turbulent premixed combustion is studied using DNS. A skeletal mechanism is employed for methane-air combustion with non-unity Lewis numbers. The reaction zones are distributed for the MILD case, and thin-sheet like for the premixed case. The instantaneous heat release rate is compared with the experimentally measurable field of $S_{\text{OH}} \times S_{\text{CH}_2\text{O}}$, and a close resemblance of these two fields is observed for both cases. The scalar gradient PDFs conditioned on the heat release rate are constructed using the PLIF-like images deduced from the DNS data. These PDFs show that the flamelet behaviour appears less in the MILD case compared to the premixed case. It seems that these PDFs can provide a robust statistical method to assess flamelet and non-flamelet turbulent combustion using laser diagnostics.

Acknowledgement

YM acknowledges the financial support of Nippon Keidanren and Cambridge Overseas Trust. EPSRC support is acknowledged by NS. This work made use of the facilities of HECToR at UoE funded by EPSRC.

References

- [1] J. A. Wüning and J. G. Wüning, "Flameless oxidation to reduce thermal NO-formation," *Prog. Energy Combust. Sci.*, vol. 23, pp. 81–94, 1997.
- [2] M. Katsuki and T. Hasegawa, "The science and technology of combustion in highly preheated air," *Proc. Combust. Inst.*, pp. 3135–3146, 1998.
- [3] A. Cavaliere and M. de Joannon, "Mild combustion," *Prog. Energy Combust. Sci.*, vol. 30, pp. 329–366, 2004.
- [4] T. Plessing, N. Peters, and J. G. Wüning, "Laseroptical investigation of highly preheated combustion with strong exhaust gas recirculation," *Proc. Combust. Inst.*, pp. 3197–3204, 1998.
- [5] I. B. Özdemir and N. Peters, "Characteristics of the reaction zone in a combustor operating at mild combustion," *Exp. Fluids*, vol. 30, pp. 683–695, 2001.
- [6] P. H. Paul and H. N. Najm, "Planar laser-induced fluorescence imaging of flame heat release rate," *Proc. Combust. Inst.*, pp. 43–50, 1998.
- [7] M. Tanahashi, S. Murakami, G. M. Choi, Y. Fukuchi, and T. Miyauchi, "Simultaneous CH-OH PLIF and stereoscopic PIV measurements of turbulent premixed flames," *Proc. Combust. Inst.*, vol. 30, pp. 1665–1672, 2005.
- [8] J. Kiefer, Z. S. Li, T. Seeger, A. Leipertz, and M. Aldén, "Planar laser-induced fluorescence of hco for instantaneous flame front imaging in hydrocarbon flames," *Proc. Combust. Inst.*, vol. 32, pp. 921–928, 2009.
- [9] S. Hayashi and Y. Mizobuchi, "Utilization of hot burnt gas for better control of combustion and emissions," in *Turbulent premixed flames*, N. Swaminathan and K. N. C. Bray, Eds. Cambridge, UK: Cambridge University Press, 2011, pp. 365–378.
- [10] Y. Minamoto, T. D. Dunstan, N. Swaminathan, and R. S. Cant, "DNS of egr-type turbulent flame in mild condition," *Proc. Combust. Inst.*, p. 10.1016/j.proci.2012.06.041, 2012.